Malitckii, Evgenii; Yagodzinskyy, Yuriy; Lehto, Pauli; Remes, Heikki; Hänninen, Hannu

Hydrogen uptake and its effect on mechanical properties of 18% Cr ferritic stainless steel

Published in:
Hydrogen Conference (IHC 2016)

DOI:
10.1115/1.861387_ch15

Published: 01/01/2017

Document Version
Peer-reviewed accepted author manuscript, also known as Final accepted manuscript or Post-print

Published under the following license:
Unspecified

Please cite the original version:
Malitckii, E., Yagodzinskyy, Y., Lehto, P., Remes, H., & Hänninen, H. (2017). Hydrogen uptake and its effect on mechanical properties of 18% Cr ferritic stainless steel. In B. P. Somerday, & P. Sofronis (Eds.), *Hydrogen Conference (IHC 2016): Materials Performance in Hydrogen Environments* American Society of Mechanical Engineers. https://doi.org/10.1115/1.861387_ch15

HYDROGEN UPTAKE AND ITS EFFECT ON MECHANICAL PROPERTIES OF 18%CR FERRITIC STAINLESS STEEL

EVGENII MALITCKII
Aalto University, Finland

YURIY YAGODZINSKYY
Aalto University, Finland

PAULI LEHTO
Aalto University, Finland

HEIKKI REMES
Aalto University, Finland

JYRKI ROMU
Aalto University, Finland

HANNU HÄNNINEN
Aalto University, Finland

ABSTRACT

Ferritic stainless steel with 18 wt% of chromium is studied in order to clarify its sensitivity to hydrogen effects. Hydrogen uptake and diffusion were analyzed using thermal desorption method. Hydrogen diffusion transport and trapping in the concentrated Fe-Cr alloy is discussed. Hydrogen effects on the mechanical properties of the steel are studied with CERT performed under continuous H-charging. Hydrogen has a remarkable effect on the elongation to fracture of the Fe-Cr ferrite: uniform elongation of the steel reduces up to 75% in presence of hydrogen. A special attention is paid to the role of grain size on the steel sensitivity to hydrogen embrittlement.

INTRODUCTION

Ferritic stainless steels are attractive materials for applications in gas and oil, automotive and marine industries due to their enhanced corrosion resistance and relatively low price compared to austenitic stainless steel grades. However, the microstructural features of the ferrite which has body-centered cubic (bcc) crystal lattice cause a significant loss in ductility as compared to that in austenitic steels having face-centered cubic (fcc) arrangement of atoms in the crystal lattice. Furthermore, the difference in packing density and crystal lattice structure makes the ferritic stainless steels more prone to formation of second phase precipitates during heat treatment resulting in increase of the ductile to brittle transition temperature (DBTT) [1]. Such heat treatment can be performed during, for instance, welding processes resulting in formation of a gradient of the microstructure through the heat-affected zone of ferritic stainless steel weldment [2]. Hydrogen trapped from both manufacturing and service environments can reduce significantly the mechanical properties of the ferritic steel. At the same time, the effects of the microstructure of ferritic stainless steel on its susceptibility to hydrogen embrittlement is the key question of the research.

Different mechanisms of the hydrogen embrittlement in the structural materials were proposed. High concentration of hydrogen may contribute in Hydrogen-enhanced decohesion (HEDE) event that usually is associated with simple sequential tensile separation of atoms when a critical crack-tip-opening displacement is reached [3, 4]. Beachem proposed hydrogen-enhanced localized

plasticity (HELP) mechanism which is based on the assumption that hydrogen is localized near crack tip due to hydrostatic stress or entry of hydrogen at crack tip facilitates dislocation activity and localization of deformation near the crack tip [5]. Hydrogen embrittlement may also be primarily the result of a high concentration of vacancies ahead of the crack tip caused by hydrogen-enhanced stress-induced vacancy (HESIV) formation [6]. The proposed theories of hydrogen embrittlement are used to describe the mechanism of quasi-cleavage fracture formation widely observed in mechanical testing of hydrogen charged ferritic stainless steels [7, 8].

This paper aims to reveal the effect of heat-treatment on the microstructure change of the ferritic stainless steel and its mechanical properties in H-free and H-charged conditions.

EXPERIMENTAL

The ferritic stainless steel (ASTM UNS S43940) was provided by Outokumpu Stainless Oyj in the shape of hot-rolled plate with a normal thickness of 3 mm. The chemical composition of the steel is shown in Table 1.

Table 1. Chemical composition of ASTM UNS S43940 ferritic stainless steel, wt%.

C	Sl	Mn	Cr	Mo	Nb	Ni	Ti	Cu	Al	V	W
0,014	0,61	0,42	17,7	0,024	0,393	0,18	0,138	0,118	0,025	0,055	0,037

Tensile specimens with gauge length of 32×5×1 mm were cut in transverse direction to the rolling plane. In order to increase the average grain size (GS) of the steel the prepared specimens were annealed at 1050ºC and 1200ºC for one hour and quenched in water. All the specimens were mechanically polished finishing with 6 μm diamond paste.

Marble`s reagent was used for etching of the annealed steel specimens after mechanical polishing finishing with 1 μm diamond paste. GS measurements were performed from optical microscopy photographs using the intercept length method [2, 9].

Electrochemical hydrogen charging was performed from 0.1N H_2SO_4 solution with 20 mg/l of thiourea ($CS(NH_2)_2$) at controlled potential of -1.2 $V_{Hg/Hg2SO4}$. Thermal desorption spectroscopy (TDS) measurements were performed with a heating rate of about 6 K/min from room temperature to 850ºC. Basic pressure of ultra-high vacuum (UHV) chamber of TDS apparatus is about 10^{-8} mbar. The size of the TDS specimens is about 7.5×3.8×1 mm. Dwelling time between the end of electrochemical hydrogen charging and starting of the TDS measurement is about 30 minutes.

Tensile tests were performed at room temperature in H-free condition and during continuous hydrogen charging using a 35 kN MTS desk-top testing machine at strain rate of 10^{-4} s^{-1}. Tensile specimens tested during continuous hydrogen charging were pre-charged with hydrogen before tensile testing for four hours that was experimentally found to be enough for a homogeneous hydrogen distribution.

RESULTS

Annealing of the tensile specimens of the studied ferritic stainless steel results in an increase of the average GS from 17 μm for as-supplied steel to 65 μm and 349 μm for specimens heat-treated at 1050°C and 1200°C, respectively. A relative grain size dispersion value was calculated from the measured distribution as follows [10]:

$$\frac{\Delta d}{d} = \frac{d_{max} - d_{min}}{d} \quad (1)$$

where, d - average GS, d_{max} and d_{min} - maximum and minimum grain sizes, respectively. The relative dispersion parameter calculated for as-supplied condition of the studied steel was 2.8. After heat treatment of the studied steel at temperature of 1050°C a minor increase of relative dispersion value of the GS distribution was observed to the value of 2.9. However, the dispersion increases significantly up to 4.6 with the increase of the annealing temperature to 1200°C.

Constant extension rate tests (CERT) of the studied ferritic stainless steel were performed first in H-free condition for as-supplied and annealed steel specimens. The obtained CERT stress-strain curves are shown in Fig. 1. The annealing procedures of the as-supplied steel specimens resulting in increase of the average GS affect significantly the mechanical properties of the steel. The elongation to fracture of about 29.3% obtained for the as-supplied steel reduces to about 27.5% and 15.7% with increase of the average grain size to 65 μm and 349 μm, respectively. Tensile strength also decreases from 428 Mpa to 395 Mpa and 368 Mpa, respectively.

While the elongation to fracture and tensile strength parameters manifest a uniform degradation of the mechanical properties of the ferritic stainless steel the effect of GS coarsening on yield stress is more complicated. The yield stress of the steel specimens tested in as-supplied condition is about 300 Mpa and it reduces to about 237 Mpa with increase of the average GS to 65 μm. Following coarsening of the grain structure of the studied steel causes an increase of the yield stress that is in controversy with Hall-Petch relationship [11, 12]. The observed phenomena are discussed later.

Hydrogen detrapping and release from the ASTM UNS S43940 ferritic stainless steel specimens were studied using TDS apparatus after electrochemical hydrogen charging for 1, 2, 4 and 18.5 h. As shown in Fig. 2 the hydrogen content increases rapidly with time of H-charging from 0 to 4 h and reaches the value of about 100 at.ppm. Continuous hydrogen charging results in almost the same value of the hydrogen concentration measured from the ferritic stainless steel specimens evidencing that the electrochemical hydrogen charging during 4 h or more in the conditions described above is associated with the equilibrium hydrogen distribution through the specimen thickness. Since the specimens with characteristic thickness of about 1 mm reach a hydrogen saturation state after electrochemical hydrogen charging at temperature of 20°C, the effective diffusion coefficient of hydrogen can be estimated [13] to be about 4.3×10^{-11} m^2 s^{-1} . The result correlates well with data reported for the same class of the material [14]. For example, the effective diffusion coefficient of AISI 430 was calculated to be about 8×10^{-11} m^2 s^{-1} for the same temperature conditions [15].

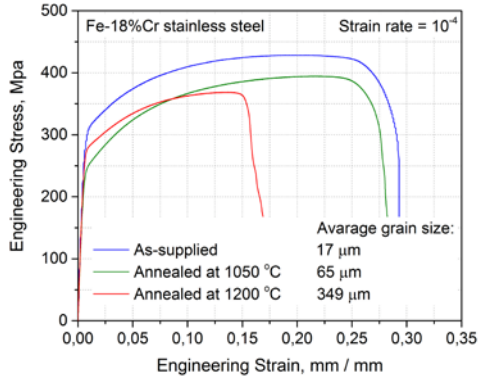

Figure 1. CERT stress-strain curves of as-supplied and annealed specimens of ASTM UNS S43940 ferritic stainless steel obtained in air with strain rate of 10^{-4} s^{-1}.

Solving the corresponding boundary problem for diffusion equation an expression for the hydrogen concentration profile can be obtained [16]:

$$C(x) = \frac{4C_0}{\pi}\sum_{n=0}^{\infty}\frac{(-1)^n}{(2n+1)}\cos\frac{(2n+1)\pi x}{h}\left(1 - e^{-\frac{\pi^2(2n+1)^2 D(T_s)t_s}{h^2}}\right)e^{-\frac{\pi^2(2n+1)^2 D(T_d)t_d}{h^2}} \qquad (2)$$

where, C_o - concentration of hydrogen on the surface, t_s and T_s - time and temperature of hydrogen charging, t_d and T_d - time and temperature of hydrogen desorption, respectively, h - thickness of the specimen, D - diffusion coefficient.

Hydrogen concentration profile after electrochemical hydrogen charging of 1 mm thick ASTM UNS S43940 stainless steel plate for 4 hours and dwelling at room temperature for 30 minutes required for starting of TDS measurement is shown in Fig. 3. The same equation was solved to estimate the hydrogen concentration profile in the studied steel directly after electrochemical hydrogen charging. The concentration of hydrogen at the final stage of the H-charging procedure was calculated to be about 290 at.ppm that is about three times higher than the measured value.

The electrochemical hydrogen charging affects markedly the mechanical properties of ASTM UNS S43940 stainless steel. Obtained CERT results manifest a significant reduction of elongation to fracture and increase of yield stress in all the specimens. The mechanical properties are summarized in Table 2.

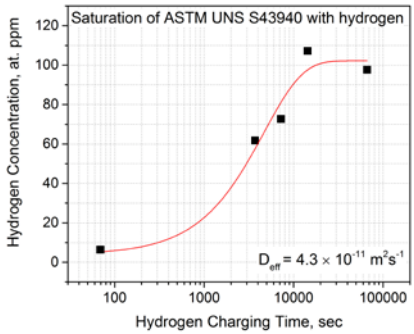

Figure 2. Relationship between hydrogen charging time and measured hydrogen concentration in the ASTM UNS S43940 ferritic stainless steel.

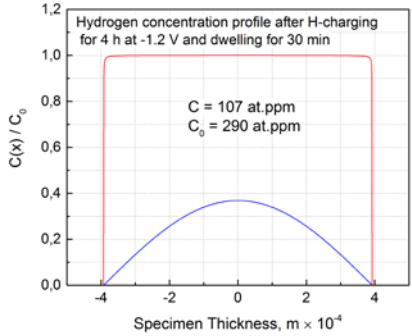

Figure 3. Hydrogen concentration profile after electrochemical hydrogen charging of 1 mm thick ASTM UNS S43940 stainless steel plate for 4 h and dwelling at room temperature for 30 min (blue) compared to calculated hydrogen concentration without dwelling (red).

Table 2. Hydrogen effect on the CERT parameters of the tensile specimens of ASTM UNS S43940 ferritic stainless steel.

GS, μm	$\frac{R_{p0.2}, MPa}{R_{p0.2H}, MPa}$	$\frac{R_m, MPa}{R_{mH}, MPa}$	$\frac{\varepsilon, \%}{\varepsilon_H, \%}$
17	$\frac{300}{371}$	$\frac{428}{437}$	$\frac{29.3}{6.9}$
65	$\frac{237}{311}$	$\frac{395}{406}$	$\frac{27.5}{7.3}$
349	$\frac{274}{350}$	$\frac{368}{372}$	$\frac{15.7}{2.5}$

The parameter of hydrogen sensitivity is defined as:

$$\delta_H = (x - x_H)/x \qquad (3)$$

where, x and x_H - CERT parameters obtained after tensile testing of H-free and H-charged tensile specimens of the studied steel. The dependence of the average GS on sensitivity to hydrogen parameters is shown in Fig. 4. The results are divided for Stage I and Stage II according to the average GS growth from 17 μm to 65 μm and from 65 μm to 349 μm, respectively. As a general observation the sensitivity to hydrogen of elongation to fracture and yield stress increase with the growth of the average GS of the studied steel. However, the detailed analysis of the results manifests a minor decrease of the deleterious effect of hydrogen on elongation to fracture at the Stage I and increase at the Stage II of the graph. For yield stress the opposite effect is observed. Only a minor effect of hydrogen on the tensile strength is observed remaining almost the same at Stage I and Stage II.

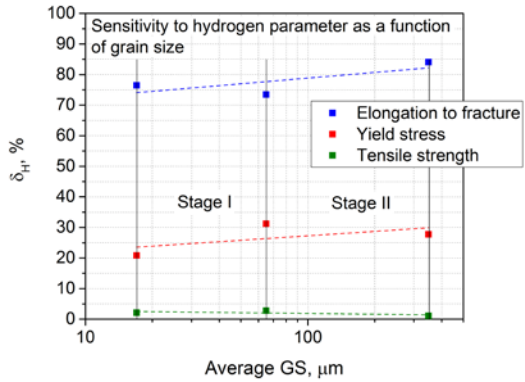

Figure 4. Sensitivity to hydrogen parameter as a function of average GS of the ASTM UNS S43940 ferritic stainless steel.

DISCUSSION

CERT test of the studied ASTM UNS S43940 ferritic stainless steel specimens tested in as-supplied condition and after annealing causing an increase of the average GS shows controversial results. The yield stress was found to increase with the average GS from 65 μm to 349 μm that does not follow the Hall-Petch relationship [11, 12]. Such a behavior is caused apparently by precipitation hardening due to presence of second-phase precipitates in the matrix that retard dislocation movement through a crystal [13]. At the same time, the increasing grain size increases the ductile to brittle transition temperature causing the brittle fracture of the steel specimens with average GS of 349 μm [13]. The microscopy of the studied steel does not reveal any change in precipitate density with increase of the annealing temperature from 1050°C to 1200°C. Decomposition of ferrite and formation of chromium-rich nanoscale clusters is also a possible reason of the steel strengthening. Chromium-rich cluster formation occurs by spinodal decomposition of ferrite to iron-rich α- and chromium-rich α′ - phases [17, 18]. Also, in characterisation of local GS variation of welded steel the increase of relative grain size dispersion $\Delta d/d$ in the heat-affected zone was attributed to decomposition of the ferrite and second-phase formation that correlate well with the obtained results [19, 20].

The diffusivity of hydrogen in α-iron is relatively high even at room temperature [21]. However, the diffusivity of hydrogen in Fe-alloys decreases with the increase of the concentration of the alloying elements due to the hydrogen trapping at the defects or crystal imperfections caused by both interstitial and substitutional atoms as well as second-phase precipitates [22-24]. Therefore, hydrogen concentration associated with homogeneous hydrogen distribution through the specimen thickness measured at about 100 at. ppm is attributed mainly to trapped hydrogen. Difference between measured hydrogen concentration and the calculated hydrogen concentration at the final stage of the hydrogen charging defines apparently the so-called diffusing hydrogen locating preferably at the

tetrahedral positions of the BCC crystal lattice as well as at the other trapping sites with low activation energies [25].

The deleterious effect of hydrogen on mechanical properties of the studied steel increases with increase of the average GS as shown in Fig. 4. The detailed observation reveals, however, a reduction of sensitivity to hydrogen on elongation to fracture in steel specimens with average GS of about 65 µm. Further increase of the sensitivity to hydrogen parameter in steel specimens with GS of about 349 µm is associated probably with a synergistic effect of both hydrogen and decomposition of the ferrite phase.

CONCLUSIONS

Hydrogen uptake and trapping of ASTM UNS S43940 ferritic stainless steel were studied after electrochemical hydrogen charging at controlled potential of -1.2 $V_{Hg/Hg2SO4}$ evidencing the hydrogen concentration of trapped hydrogen is about 100 at.ppm. The concentration of hydrogen after pre-charging for 4 hours was calculated to be about 290 at.ppm that is about three times higher than the measured value. The effective diffusivity of hydrogen in the studied steel is almost one hundred times slower as compared with a pure iron [26].

Hydrogen reduces significantly the elongation to fracture of the studied steel specimens tested in CERT during continuous hydrogen charging, while the yield stress was found to increase in the presence of hydrogen. Sensitivity to hydrogen parameter on elongation to fracture and yield stress increases with increase of the average GS of the steel specimens. But the effect of hydrogen on tensile strength remains almost the same.

ACKNOWLEDGMENTS

The ASTM UNS S43940 ferritic stainless steel was provided by Outokumpu Stainless Oyj for the research. The research was partly supported by Aalto University.

REFERENCES

1 R.A. Lula, Toughness of ferritic stainless steels, ASTM San Francisco, Calif. (1979).
2 H. Remes, P. Lehto, J. Romanoff, Microstructure and strain-based fatigue life approach for high-performance welds, Advan. Mater. Res., vol. 891-892, pp. 1500-1506 (2014).
3 A.R. Troiano, “The role of hydrogen and other interstitials on the mechanical behavior of metals”, Trans. Am. Soc. Met., vol. 53, pp. 54-80 (1960).
4 R.A. Oriani, R.H. Josephic, “Equilibrium aspects of hydrogen-induced cracking of steels”, Acta Mater., vol. 22, pp. 1065-74 (1974).
5 C.D. Beachem, “A new model for hydrogen assisted cracking (hydrogen embrittlement)”, Metall. Trans., vol. 3, pp. 437-451 (1972).
6 M. Nagumo, “Hydrogen related failure of steels – a new aspect”, Mater. Sci. Tech., vol. 20, pp. 940-50 (2004).
7 M.L. Martin, I.M. Robertson, P. Sofronis, “Interpreting hydrogen-induced fracture surfaces in terms of deformation processes: A new approach”, Acta Mater., vol. 59, pp. 3680-3687 (2011).

8 T. Neeraj, R. Srinivasan, J. Li, "Hydrogen embrittlement of ferritic steels: Observations on deformation microstructure, nanoscale dimples and failure by nanovoiding", Acta Mater., vol. 60, pp. 5160-5171 (2012).

9 ATSM-E1382-97. Standard test methods for determining average grain size using semiautomatic and automatic image analysis. West Conshohocken (PA): ASTM International, (2007).

10 S. Berbenni, V. Favier, M. Berveiller, "Micro-macro modelling of the grain size distribution on the plastic flow stress of heterogeneous materials", Comput. Mater. Sci., vol. 39, pp. 96-105 (2007).

11 E.O. Hall, "The deformation and ageing of mild steel: III Discussion of results", Proc. Phys. Soc., vol. B64, pp. 747-53 (1951).

12 N.J. Petch, "The cleavage strength of polycrystals", J. Iron Steel Inst., vol. 174, pp. 25-8 (1953).

13 R.E. Reed-Hill, R. Abbaschian, Physical Metallurgy Principles, 3rd ed., PWS-KENT Publishing Company, Boston (1991).

14 D.J. Fisher, "Hydrogen diffusion in metals. A 30-year retrospective", Hobbs Printers Ltd, Totton Hampshire SO40 3WX (1999).

15 C.H. Tseng, W.Y. Wei, J.K. Wu, "Electrochemical methods for studying hydrogen diffusivity, permeability, and solubility in AISI 420 and AISI 430 stainless steels", Mat. Sci. and Tech., vol. 5, pp. 1236-1239 (1989).

16 Y. Yagodzinskyy, O. Todoshchenko, S. Papula, H. Hänninen, "Hydrogen solubility and diffusion in austenitic stainless steels studied with thermal desorption spectroscopy", Steel Research Int., vol. 82, No 1, pp. 20-25 (2011).

17 T.J. Marrow, "The fracture mechanism in 475ºC embrittled ferritic stainless steels, Fatigue and Fracture of Engineering Materials and Structures", Issue 19, pp. 919-933 (1996).

18 P. Hedström, F. Huyan, J. Zhou, S. Wessman, M. Thuvander, J. Odqvist, "The 475ºC embrittlement in Fe-20Cr and Fe-20Cr-X (X=Ni, Cu, Mn) alloys studied by mechanical testing and atom probe tomography", Materials Science & Engineering, vol. A574, pp. 123-129 (2013).

19 P. Lehto, "Characterization of average grain size and grain size distribution", Aalto University Wiki, (2016).

20 P. Lehto, J. Romanoff, H. Remes, T. Sarikka, "Characterisation of local grain size variation of welded structural steel", Weld World, vol. 60, pp. 673-688 (2016).

21 M.Y. Solar, R.I.L. Guthrie, "Hydrogen diffusivities in molten iron between 0.1 and 1.5 atm H_2", Met. Trans., vol. 2, pp. 457-64 (1971).

22 R.A. Oriani, "The diffusion and trapping of hydrogen in steels", Acta Met., vol. 18, pp. 147-157 (1970).

23 K. Ono, L.A. Rosales, "The anomalous behavior of hydrogen in iron at lower temperature", Trans. Met. Soc., AIME, vol. 242, pp. 244-248 (1968).

24 G.M. Pressouyre, "A classification of hydrogen traps in steel", Met. Trans., vol. 10A, pp. 1571-1573 (1979).

25 J. Song, W.A. Curtin, "Atomic mechanism and prediction of hydrogen embrittlement in iron", Nat. Mater., vol. 12, pp. 145-151 (2012).

26 K.T. Kim, J.K. Park, J.Y. Lee, S.H. Hwang, "Effect of alloying elements on hydrogen diffusivity in α-iron", J. Mat. Sci., vol. 16, pp. 2590-2596 (1981).